Geophysical Research Letters

RESEARCH LETTER
10.1029/2019GL083073

Key Points:
- The AMOC at 26° N and New England coastal sea level are anticorrelated across intraseasonal and interannual timescales during 2004–2017
- This anticorrelation reflects distinct local oceanic responses to temporally correlated, spatially disparate atmospheric forcing mechanisms
- The relevant local atmospheric forcing is related to the North Atlantic Oscillation, Arctic Oscillation, and West Atlantic Index

Supporting Information:
- Supporting Information S1

Correspondence to:
C. G. Piecuch,
cpiecuch@whoi.edu

Citation:
Piecuch, C. G., Dangendorf, S., Gawarkiewicz, G. G., Little, C. M., Ponte, R. M., & Yang, J. (2019). How is New England coastal sea level related to the Atlantic meridional overturning circulation at 26° N? *Geophysical Research Letters, 46*, 5351–5360. https://doi.org/10.1029/2019GL083073

Received 29 MAR 2019
Accepted 21 APR 2019
Accepted article online 1 MAY 2019
Published online 20 MAY 2019

How is New England Coastal Sea Level Related to the Atlantic Meridional Overturning Circulation at 26° N?

Christopher G. Piecuch[1], Sönke Dangendorf[2], Glen G. Gawarkiewicz[1], Christopher M. Little[3], Rui M. Ponte[3], and Jiayan Yang[1]

[1]Physical Oceanography Department, Woods Hole Oceanographic Institution, Woods Hole, MA, USA, [2]Forschungsinstitut Wasser und Umwelt, Universität Siegen, Siegen, Germany, [3]Atmospheric and Environmental Research, Inc., Lexington, MA, USA

Abstract Monthly observations are used to study the relationship between the Atlantic meridional overturning circulation (AMOC) at 26° N and sea level (ζ) on the New England coast (northeastern United States) over nonseasonal timescales during 2004–2017. Variability in ζ is anticorrelated with AMOC on intraseasonal and interannual timescales. This anticorrelation reflects the stronger underlying antiphase relationship between ageostrophic Ekman-related AMOC transports due to local zonal winds across 26° N and ζ changes arising from local wind and pressure forcing along the coast. These distinct local atmospheric variations across 26° N and along coastal New England are temporally correlated with one another on account of large-scale atmospheric teleconnection patterns. Geostrophic AMOC contributions from the Gulf Stream through the Florida Straits and upper-mid-ocean transport across the basin are together uncorrelated with ζ. This interpretation contrasts with past studies that understood ζ and AMOC as being in geostrophic balance with one another.

1. Introduction

This paper concerns the relationship between coastal sea level and large-scale ocean circulation. Motivated by concerns over climate change and coastal vulnerability, recent studies examine sea level on the U.S. northeast coast and its relation to the Atlantic meridional overturning circulation (AMOC). The AMOC—formally defined in terms of zonally integrated mass stream function—characterizes the northward transport of warmer waters near the surface and southward return flow of cooler waters at depth in the Atlantic Ocean, which plays an important role in climate (Buckley & Marshall, 2016). Models show that, over a range of timescales, AMOC strength is anticorrelated with sea level on the New England coast, between New York City and the Canada-U.S. border (Bingham & Hughes, 2009; Hu & Bates, 2018; Landerer et al., 2007; Little et al., 2017; Yin et al., 2009). Yin et al. (2009) find that, in future climate model projections, a centennial decline in AMOC stream function at 45° N is accompanied by enhanced sea level rise in New York City and Boston related to ocean dynamics. This finding is interpreted in terms of geostrophy—a weakening of the Gulf Stream or North Atlantic Current is balanced by an increase in sea level at the coast. Considering an ocean general circulation model spanning 1985–2004, Bingham and Hughes (2009) determine that changes in coastal sea level from New York City to Yarmouth are in antiphase with changes in northward upper-ocean (100–1,300 m) volume transport at 50° N in the North Atlantic Ocean on interannual timescales. This result is explained in terms of geostrophic balance, applied zonally across the basin—if the eastern boundary condition is negligible, and coastal sea level on the western boundary varies coherently with bottom pressure on the shelf and slope, then western boundary coastal sea level and northward volume transport are in antiphase.

While apparent in models, such relationships between AMOC and New England coastal sea level have been more difficult to detect in observations. Some studies suggest that the imprints of AMOC changes are evident in historical sea level records along the New England coast; however, many of these suggestions are tenuous, based on qualitative comparisons between observed and modeled sea level-rise patterns (Sallenger et al., 2012), or relationships assumed between AMOC and modes of multidecadal climate variability (Kopp, 2013). Direct observational links between coastal sea level and AMOC have, until recently, been lacking.

Contrasting interannual changes in tide-gauge records on the New England coast with AMOC observations from the RAPID monitoring array at 26° N in the Atlantic during 2004–2012, Goddard et al. (2015) reveal that coastal sea level is anticorrelated with the AMOC, most notably during 2009–2010, when the AMOC temporarily weakened by 30% at the same time that sea level rose by about 10 cm along the New England coast. Those authors reason that the coastal sea level rise over 2009–2010 was caused by the 30% AMOC downturn in combination with wind forcing related to a strong negative North Atlantic Oscillation (NAO) event. The Goddard et al. (2015) analysis prompts a number of questions. They consider a relatively short AMOC time series and are mainly interested in a particular event. It remains to determine how coastal New England sea level corresponds to AMOC more generally as a function of time and frequency, now that a longer AMOC record from the RAPID program has become available (extending into 2017). Goddard et al. (2015) also posit that the AMOC decline was in part causally responsible for the sea level rise. However, the nature of the relationship between these two quantities—whether indicating correlation or causation—and the underlying mechanisms is still to be firmly established.

Volkov et al. (2018) report an antiphase relationship between AMOC at 26° N and sea level in the Mediterranean Sea over 2004–2017, which they explain in terms of a large-scale atmospheric teleconnection. During positive NAO states, stronger trade winds drive enhanced northward Ekman transports across 26° N in the Atlantic, increasing the strength of the AMOC. At the same time, anomalous easterlies along the Strait of Gibraltar force flow out of the Mediterranean, leading to a wind setup, which lowers average sea level over the Mediterranean. The reverse occurs during negative NAO states, with AMOC weakening at 26° N and sea level increasing over the Mediterranean (Volkov et al., 2018). Since previous studies highlight the influence of local air pressure and alongshore winds (partly tied to the NAO) in driving sea level changes on the New England coast (Andres et al., 2013; Kenigson et al., 2018; Li et al., 2014; Noble, 1979; Piecuch & Ponte, 2015; Piecuch et al., 2016; Sandstrom, 1980; Thompson, 1986; Woodworth et al., 2014), it stands to reason that instances of anticorrelation between New England coastal sea level and AMOC monitored at 26° N could result from a similar teleconnection process.

We address two questions. First, over what frequency bands and during what time periods is a significant coherence found between observations of New England coastal sea level and the AMOC at 26° N? Second, what processes are responsible for instances of significant coherence? Given the data availability (next section), we restrict our exploration of these questions to intraseasonal and interannual timescales during 2004–2017.

2. Data

2.1. Overturning Circulation

We use the AMOC time series at 26° N (T_{moc}) from the RAPID monitoring program (McCarthy et al., 2015). The RAPID array is designed such that T_{moc} represents the northward flow above ~1,100 m due to the Gulf Stream in the Florida Straits measured by undersea cables between Florida and the Bahamas (T_{gs}), the Ekman transport at 26° N derived from reanalysis zonal wind stress across the basin (T_{ek}), and the upper mid-ocean transport between the Bahamas and Morocco (T_{umo}),

$$T_{moc} = T_{gs} + T_{ek} + T_{umo}. \tag{1}$$

The upper mid-ocean transport includes contributions from the Antilles Current and Deep Western Boundary Current measured by current meters between Abaco and 76.75° W (T_{wbw}), the basin-wide interior geostrophic flow monitored by dynamic height moorings between 76.75° W, and the Moroccan coast (T_{int}), along with an external transport included to maintain mass balance (T_{ext}),

$$T_{umo} = T_{wbw} + T_{int} + T_{ext}. \tag{2}$$

Thus, the sum $T_{gs} + T_{umo}$ essentially represents the geostrophic component of the AMOC. See McCarthy et al. (2015) for more details on monitoring the AMOC at 26° N. As of this writing, 12-hourly time series of 3-day-smoothed T_{moc} and its components are available from April 2004 to February 2017 at the RAPID website.

2.2. Sea Level

We use monthly tide-gauge relative sea level (ζ) records from the Permanent Service for Mean Sea Level Revised Local Reference database (Holgate et al., 2013; Permanent Service for Mean Sea Level (PSMSL), 2018). We consider ζ data from eight New England stations (Table S1 and Figure S1 in the supporting information). Our decision to focus specifically on the New England coast, rather than more generally along the North American northeast coast, was motivated by previous observational studies of the relationship between coastal sea level and the large-scale circulation. Bingham and Hughes (2009) identify a set of 10 tide-gauge records from New York City to Yarmouth that are most representative of the leading mode of interannual sea level variability based on satellite altimetry over the eastern North American shelf from 35° N to 55° N. Goddard et al. (2015) reveal that, contemporaneous with a 30% downturn in the AMOC during 2009–2010, sea level rose much faster at 13 tide gauges from Montauk to Halifax than anywhere else on the U.S. east coast during that time period. The tide gauges selected here represent most of the data records shared in common between Bingham and Hughes (2009) and Goddard et al. (2015).

The tide-gauge records are mostly complete, with ≥96% data coverage during 2004–2017, but the few gaps are filled using spline interpolation. No adjustments are made to the data (e.g., to remove the influences of glacial isostatic adjustment or the inverted barometer effect). The ζ records are strongly correlated (Figure S2), so we average them together to reduce dimensionality and produce a regional composite ζ time series. Our analysis focuses on this regional average ζ time series, but results are robust and insensitive to this choice. Very similar results were found from considering the individual tide gauges, or other data along open ocean stretches of coastline from Cape Hatteras to Atlantic Canada (Figures S3–S6), indicating the large spatial scales of ζ variability.

2.3. Atmospheric Forcing

To interpret the data, we use monthly regular 0.75° × 0.75° latitude-by-longitude grids of sea level pressure (p_a) and surface wind stress ($\vec{\tau}$) from the European Centre for Medium-Range Weather Forecasts Reanalysis Interim (ERA-Interim) covering from 1979 to present (Dee et al., 2011). We interpolate the ERA-Interim grids to the tide gauge locations and, as with the ζ data, average the time series together, resulting in regional p_a and $\vec{\tau}$ composites used in subsequent analysis. Note that we also considered p_a and $\vec{\tau}$ grids from the National Centers for Environmental Prediction-National Center for Atmospheric Research Reanalysis 1 (Kalnay et al., 1996; Kistler et al., 2001) and found practically identical results (Table S2; Figures S7 and S8).

2.4. Data Processing

We focus on aperiodic behavior during the period common to all data sets. We consider monthly averages of all time series from May 2004 to January 2017, removing simultaneous fits of linear trends and seasonal cycles using least squares. Statistical significances and error estimates for correlations, regressions, and wavelets are estimated using repeated simulations with synthetic time series and Fourier phase scrambling (Piecuch et al., 2017). All ± values quoted in the text represent 95% confidence intervals, and $p < 0.05$ and $p < 0.01$ indicate statistical significance at the 95% and 99% confidence levels, respectively.

3. Results

3.1. Relationship Between T_{moc} and ζ

Past works consider the connection between low-pass-filtered T_{moc} and ζ records during the shorter 2004–2012 interval (Goddard et al., 2015). We revisit the relationship between these two quantities more generally using monthly data over the longer 2004–2017 period. Time series of T_{moc} and ζ are shown in Figure 1a. The two quantities show clear instances of anticorrelated variation, such that ζ increases when T_{moc} decreases, and vice versa. On shorter intraseasonal scales, spikes of $\gtrsim$7 cm in ζ co-occur with drops of $\gtrsim$6 Sv in T_{moc} in January–February 2010, December 2010, and March 2013 (1 Sv $\doteq 10^6$ m^3/s). Over longer interannual periods, a subtle T_{moc} decline of ~5 Sv and ζ rise of ~9 cm between 2006 and 2010 were gradually followed by partial recoveries in both quantities, such that ζ decreased by ~8 cm and T_{moc} increased by ~2 Sv during 2011–2015. The correlation coefficient between T_{moc} and ζ is $r = -0.49$, which is statistically significant ($p < 0.01$). Correlation remains significant, albeit slightly weaker, if the prominent variations during 2009–2010 highlighted by Goddard et al. (2015) are omitted ($r = -0.38$, $p < 0.01$). Introducing leads or lags into the time series results in weaker, less significant correlations (Figure S9a), suggesting a true antiphase correspondence between the two quantities.

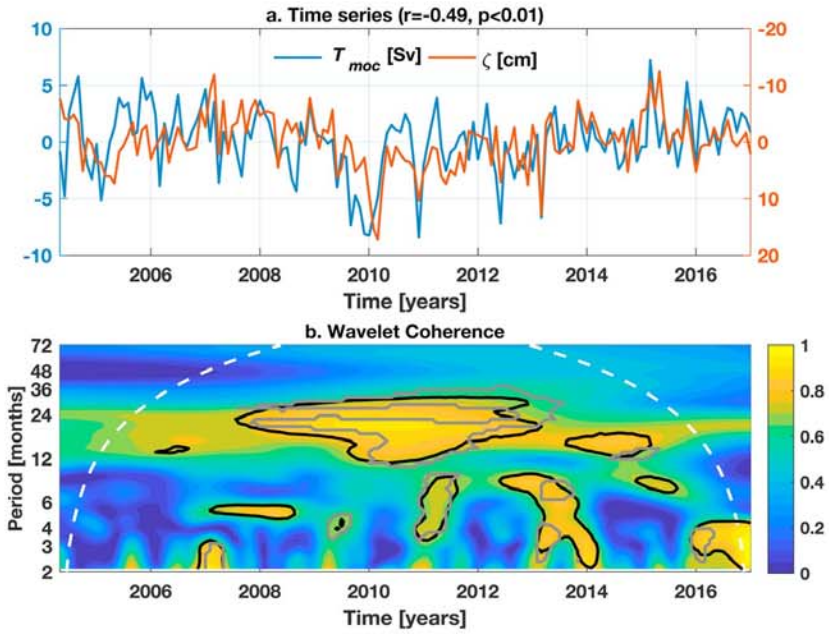

Figure 1. (a) Monthly time series of T_{moc} from the RAPID program at 26° N (Sv; blue) and ζ on the New England coast based on tide gauge data (cm; orange) from May 2004 to January 2017. Linear trends and seasonal cycles were removed from both curves. Note the inverted vertical axis on the ζ time series. (b) Magnitude-squared wavelet coherence between the T_{moc} and ζ time series. White dashes mark the cone of influence, and black lines denote values significant at the $p < 0.05$ level. Gray lines mark instances when all of the following are true at the $p < 0.05$ level: T_{ek} is coherent with ζ_{loc}, T_{moc} is coherent with T_{ek}, and ζ is coherent with ζ_{loc} (cf. Figures 2b, S13a, and S14a).

To examine the relationship between T_{moc} and ζ more systematically, we compute their wavelet coherence (Grinsted et al., 2004), which is a generalized measure of correlation in time-frequency space. The wavelet coherence structure is complex, and there are multiple instances of significant coherence between T_{moc} and ζ at intraseasonal and interannual timescales (Figure 1b). Considering lower-frequency behavior, we see that fluctuations in T_{moc} and ζ with 1- to 3-year periods centered between late 2007 and late 2013, including the 2009–2010 interannual event discussed by Goddard et al. (2015), and 1- to 2-year periods from early 2013 to late 2014 are significantly coherent. With respect to higher-frequency vacillations, significant coherence between T_{moc} and ζ is clearest at 2- to 12-month periods between mid-2012 and early 2014, but also for 2- to 4-month periods in late 2006 and early 2007, 6- to 12-month periods centered on early 2011, and 2- to 6-month periods during 2016. Considering phase angles from the cross wavelet transform during instances of significant coherence between T_{moc} and ζ (and outside the cone of influence in Figure 1b), we compute a circular mean phase angle of 179° and standard deviation of 21°, consistent with the 180° value expected for antiphase correspondence (not shown). These results establish that T_{moc} and ζ varied coherently in antiphase, not only during an interannual event between 2009 and 2010 but also more generally during 2004–2017 across a range of timescales.

3.2. Mediating Processes

What processes are responsible for the correspondence between T_{moc} and ζ (Figure 1)? To elucidate the physics, we use multiple linear regression to partition ζ,

$$\zeta = \underbrace{\alpha\, p_a + \beta\, \tau_{\parallel}}_{\zeta_{loc}} + \zeta_{res}, \tag{3}$$

where $\tau_{\parallel} \doteq \tilde{n}_{\parallel} \cdot \vec{\tau}$ is the alongshore projection of $\vec{\tau}$, where $\tilde{n}_{\parallel} \doteq (\cos\phi, \sin\phi)$ and ϕ is the coastal orientation in longitude and latitude. Following Andres et al. (2013), we choose $\phi = 30°$, but results are insensitive to reasonable alternative choices of ϕ (Figure S10). In equation (3), ζ_{loc} is meant to capture the ζ response to local p_a and $\tau_{\parallel}$ variation, while ζ_{res} is designed to absorb any other uncorrelated ζ drivers (e.g., remote forcing by other mechanisms). We compute regression coefficients of $\alpha = (-1.06 \pm 0.45) \times 10^{-4}$ m/Pa and

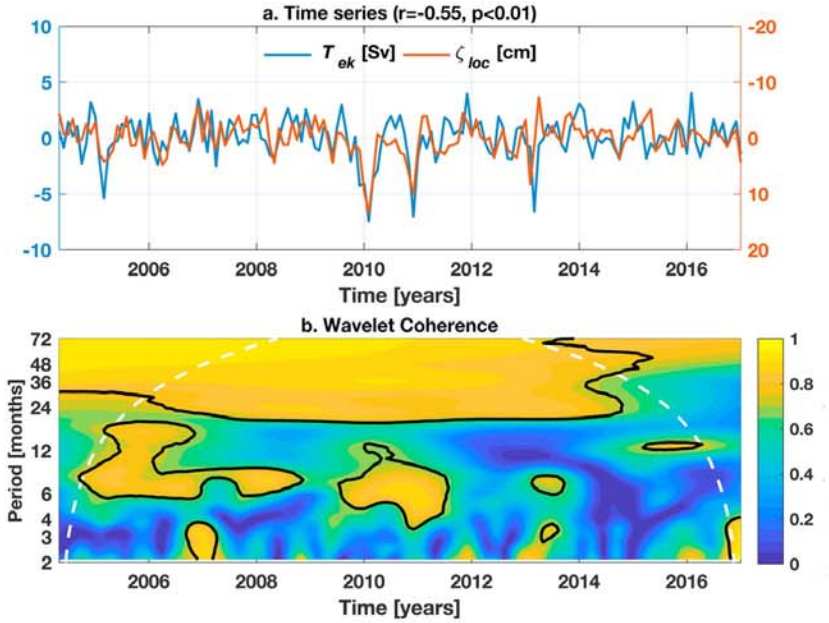

Figure 2. (a) Monthly time series of T_{ek} from the RAPID program at 26° N (Sv; blue) and ζ_{loc} on the New England coast based on tide gauge data (cm; orange) from May 2004 to January 2017. Linear trends and seasonal cycles were removed from both curves. Note the inverted vertical axis on the ζ_{loc} time series. (b) Magnitude-squared wavelet coherence between the T_{ek} and ζ_{loc} time series. White dashes mark the cone of influence, and black lines denote values significant at the $p < 0.05$ level.

$\beta = (-0.42 \pm 0.25)$ m^3/N. Note that p_a and $\tau_{\parallel}$ are uncorrelated ($r = 0.17$, $p > 0.05$) and constitute independent regressors. The value computed for α is consistent with the regression coefficient expected between ζ and p_a for a local inverted barometer response, which represents the ocean's isostatic adjustment to local p_a (Wunsch & Stammer, 1997). The calculated β value is consistent with the transfer function between $\tau_{\parallel}$ and ζ anticipated from a simple barotropic coastal model that envisions an alongshore momentum balance between wind stress and bottom friction, and an offshore momentum balance between the offshore ζ gradient and a coastal-trapped alongshore current (Sandstrom, 1980), assuming representative values of friction coefficient and offshore decay scale (Andres et al., 2013). Therefore, while α and β are determined from statistical regression, their numerical values have clear physical interpretations in terms of locally forced coastal ocean dynamics.

We entertained an alternate model incorporating onshore wind stress $\tau_{\perp} \doteq \tilde{n}_{\perp} \cdot \vec{\tau}$ as an additional regressor contributing to ζ_{loc}, where $\tilde{n}_{\perp} \doteq (-\sin\phi, \cos\phi)$. Note that $\tau_{\perp}$ is uncorrelated with both p_a and $\tau_{\parallel}$. Including $\tau_{\perp}$ in the regression had no impact on the results, and the regression coefficient on $\tau_{\perp}$ was indistinguishable from zero (Table S2; Figures S11 and S12). That $\tau_{\perp}$ forcing is unimportant here is not because $\tau_{\perp}$ cannot in principle drive ζ changes (e.g., through wind setup; Csanady, 1982), but rather because $\vec{\tau}$ has a weak onshore projection over the study region (cf. Figure 4).

To assess the contribution of local forcing to the relationship between T_{moc} and ζ (Figure 1), we consider T_{ek} and ζ_{loc} time series in Figure 2a. Note that ζ_{loc} explains 41% of the ζ variance and T_{ek} explains 39% of the T_{moc} variance on nonseasonal monthly timescales during 2004–2017, consistent with past studies arguing that local forcing contributes importantly to ζ and T_{moc} variability on these timescales (e.g., Andres et al., 2013; Heimbach et al., 2011; Kenigson et al., 2018; Li et al., 2014; Piecuch & Ponte, 2015; Piecuch et al., 2016; Pillar et al., 2016; Woodworth et al., 2014; Zhao & Johns, 2014). For example, Woodworth et al. (2014) argue that local winds are a dominant driver of interannual sea level variability along the northeast American Atlantic coast. More relevant for our purposes, T_{ek} and ζ_{loc} are strongly anticorrelated with one another ($r = -0.55$, $p < 0.01$). The correlation between T_{ek} and ζ_{loc} is stronger than between T_{moc} and ζ, hinting that the relationship between T_{moc} and ζ owes to the stronger underlying correspondence between T_{ek} and ζ_{loc}. Visually inspecting the time series, we infer that T_{ek} and ζ_{loc} are in antiphase, such that ζ_{loc} rises at the same time that T_{ek} weakens. Examples include January–March 2010 and November–December 2010, when T_{ek} decreased

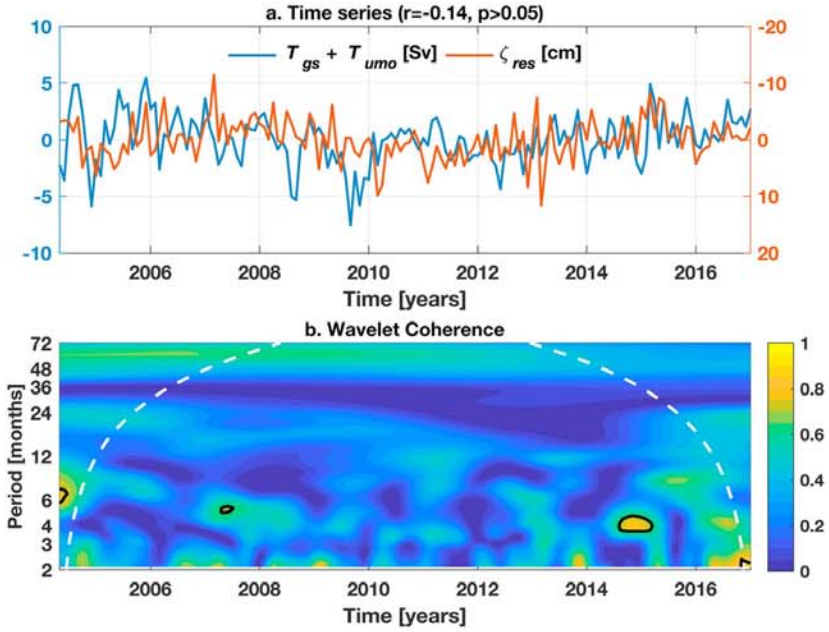

Figure 3. (a) Monthly time series of $T_{gs} + T_{umo}$ from the RAPID program at 26° N (Sv; blue) and ζ_{res} on the New England coast based on tide gauge data (cm; orange) from May 2004 to January 2017. Linear trends and seasonal cycles were removed from both curves. Note the inverted vertical axis on the ζ_{res} time series. (b) Magnitude-squared wavelet coherence between the $T_{gs} + T_{umo}$ and ζ_{res} time series. White dashes mark the cone of influence and black lines denote values significant at the $p < 0.05$ level.

by $\gtrsim$2 Sv and ζ_{loc} increased by $\gtrsim$5 cm, but also February–March 2005, April–June 2008, and February–March 2013, when ζ_{loc} rose and T_{ek} weakened by lesser amounts. Instances of simultaneously strong T_{ek} and low ζ_{loc} are also evident (e.g., April–June 2008, February–March 2013, September–October 2014, and June–July 2015). Lagged correlation analysis corroborates the inference of an antiphase relation, showing that leading or lagging ζ_{loc} relative to T_{ek} reduces and renders insignificant the correlation (Figure S9b).

To comprehensively identify instances of significant correspondence between T_{ek} and ζ_{loc}, we consider their wavelet coherence (Figure 2b). Significant coherence appears broadly at lower interannual frequencies. Instances of significant coherence are also apparent at higher intraseasonal frequencies, such as 4- to 12-month periods between late 2009 and early 2011, reflecting the sharp ζ_{loc} rise and T_{ek} drop during January–March 2010 and November–December 2010 (Figure 2a), and 6- to 18-month periods between late 2004 and mid-2008. Phase angles between T_{ek} and ζ_{loc} are essentially identical to those between T_{moc} and ζ, pointing to an antiphase relationship (not shown), but coherence between T_{ek} and ζ_{loc} is stronger and more significant than between T_{moc} and ζ (Figures 1b and 2b). Differences between the wavelet coherence spectra (Figures 1b and 2b) are clarified by considering wavelet coherence spectra between ζ and ζ_{loc} and between T_{moc} and T_{ek} (Figures S13a and S14a). Most instances of significant coherence between T_{moc} and ζ are such that, not only are T_{ek} and ζ_{loc} coherent but so are ζ and ζ_{loc} and also T_{moc} and T_{ek} (Figures 1b, 2b, S13a, and S14a). In other words, times when ζ and T_{moc} are coherent largely correspond to those times when ζ_{loc} controls ζ, T_{ek} governs T_{moc}, and ζ_{loc} and T_{ek} vary in antiphase (Figure 1b). In contrast, when any of $T_{gs} + T_{umo}$ and ζ_{res}, ζ and ζ_{res}, or T_{moc} and $T_{gs} + T_{umo}$ are significantly coherent, the coherence between T_{moc} and ζ tends to be low and insignificant (cf. Figures 3b, S13b, and S14b).

To explore this notion in more depth, we plot $T_{gs} + T_{umo}$ and ζ_{res} in Figure 3a, seeing whether the other AMOC components show meaningful correspondence to the remaining sea level signal at the coast. In contrast to earlier comparisons (Figures 1 and 2), visual inspection yields no obvious relation between $T_{gs} + T_{umo}$ and ζ_{res}. Indeed, correlation coefficients between ζ_{res} and any of $T_{gs} + T_{umo}$ ($r = -0.14$), T_{gs} ($r = -0.11$), and T_{umo} ($r = -0.04$), or between $T_{gs} + T_{umo}$ and ζ ($r = -0.20$) or ζ_{loc} ($r = -0.13$), are all statistically insignificant ($p > 0.05$). A lagged correlation analysis suggests a marginally significant anticorrelation between ζ_{res} and $T_{gs} + T_{umo}$ when the former leads the latter by ~20 months (Figure S9c), but it is unclear whether this results from random chance, given the uncertainties. To probe further and test for isolated cases of significant

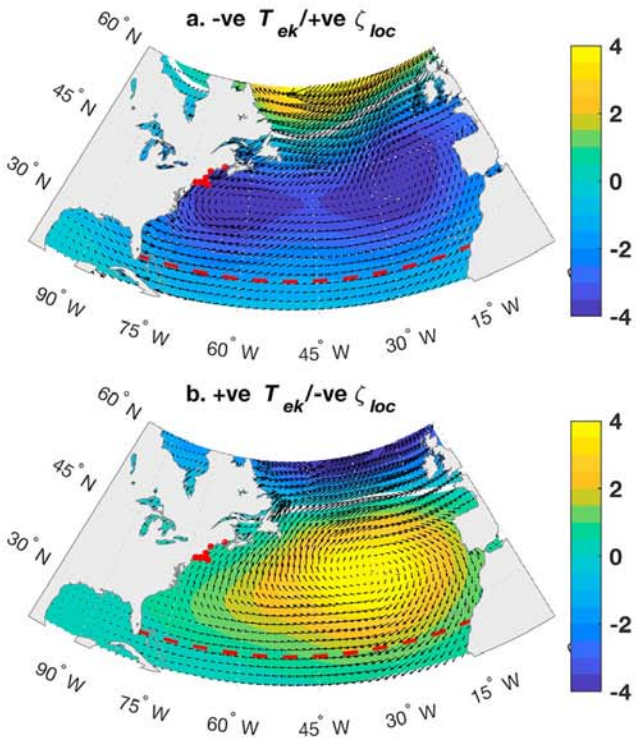

Figure 4. (a) Composite of anomalous p_a (shading; hPa) and $\vec{\tau}$ (arrows) during periods of simultaneously weak T_{ek} and high ζ_{loc} from Figure 2a (more than one respective standard deviation from the mean). White line is the p_a zero crossing. Red dots are the locations of the eight tide gauges used here (Table S1), and red dashes mark the RAPID line at 26° N. As in (a) but for periods of simultaneously strong T_{ek} and low ζ_{loc} from Figure 2a.

correspondence, we show the wavelet coherence between $T_{gs} + T_{umo}$ and ζ_{res} in Figure 3b. An instance of significant coherence is seen for 4- to 6-month periods late in 2014, but overall coherence is low and insignificant.

Based on Figures 1–3, we conclude that coherence between T_{moc} and ζ results from local atmospheric forcing, occurring when T_{ek} changes due to zonal $\vec{\tau}$ fluctuations across 26° N control T_{moc} variations and are anticorrelated with ζ_{loc} fluctuations owing to variable p_a and $\tau_{\parallel}$ along the coast that govern ζ changes.

3.3. Relation to Large-Scale North Atlantic Surface Climate

What underlies the relationship between T_{ek} and ζ_{loc} (Figure 2)? To give some broader context, and clarify how local forcing relates to surface climate more generally, we briefly consider p_a and $\vec{\tau}$ composites over the North Atlantic. Figure 4a shows p_a and $\vec{\tau}$ values averaged over months when both ζ_{loc} is more than one standard deviation higher and T_{ek} more than one standard deviation weaker than the respective mean value during 2004–2017, whereas Figure 4b maps p_a and $\vec{\tau}$ fields averaged over times when both ζ_{loc} is at least one standard deviation lower and T_{ek} at least one standard deviation stronger than the mean.

When T_{ek} is comparatively weak and ζ_{loc} high, anomalous cyclonic (counterclockwise) $\vec{\tau}$ encircles a broad anomalous low p_a system spanning the subtropical North Atlantic (Figure 4a). The spatial structure suggests two p_a centers of action, one to the east centered on 41° N, 24° E around the Azores High, another to the west centered on 39° N, 65° W. The trade winds are weakened, consistent with southward T_{ek} anomalies at 26° N, and anomalous northeasterlies appear along the New England coast, consonant with increased ζ_{loc} and associated onshore transports. The low p_a system facilitates further ζ_{loc} rise, exacerbating the ζ_{loc} increase due to $\vec{\tau}$ forcing. In contrast, when T_{ek} is relatively strong and ζ_{loc} low, anticyclonic (clockwise) $\vec{\tau}$ anomalies accompany an unusually high p_a system across the subtropical North Atlantic, with a single center of action focused on 39° N, 31° E over the Azores (Figure 4b). Strengthened trade winds drive enhanced northward T_{ek} values across 26° N at the same time that high p_a and southwesterly $\vec{\tau}$ conspire to reduce ζ_{loc} at the coast. In both cases, there is minimal onshore projection of $\vec{\tau}$ along the coast (Figure 4), in agreement with our earlier argument that $\tau_{\perp}$ forcing is unimportant in the present context.

The p_a and $\vec{\tau}$ distributions associated with periods of anomalous T_{ek} and ζ_{loc} values (Figure 4), especially the p_a centers of action near the Azores High, are reminiscent of the NAO (Hurrell, 1995), West Atlantic Index (Kenigson et al., 2018), and Arctic Oscillation (Thompson & Wallace, 1998) teleconnection patterns (cf. Figure S15). Both T_{ek} and ζ_{loc} are significantly correlated with each of these large-scale climate modes (Table S3), and a multiple linear regression performed using the time series from these teleconnection patterns as the regressors explains 48% and 53% of the variance in T_{ek} and ζ_{loc}, respectively (not shown). (Note that these modes are correlated with one another and are not independent regressors.) Performing a partial correlation analysis, after removing the influences of these teleconnection patterns as determined through multiple linear regression, we find that T_{ek} and ζ_{loc} are uncorrelated ($r = -0.11$, $p > 0.05$). This finding reveals that the anticorrelation between T_{ek} and ζ_{loc} results from Northern Hemisphere teleconnection patterns.

4. Discussion

We used observations to study the relationship between New England coastal sea level and the AMOC at 26° N on nonseasonal monthly timescales during 2004–2017. We found a significant anticorrelation between these two quantities, which reflects coherence between sea level and the overturning circulation at intraseasonal and interannual timescales during the study period (Figure 1). This correspondence results from coastal sea level anomalies driven by local alongshore wind and air pressure that arise at the same time that

anomalous Ekman transports occur from variable zonal wind stress along 26° N (Figure 2). Fluctuations in the Gulf Stream through the Florida Straits and the upper mid-ocean transport between the Bahamas and Morocco together do not contribute to the anticorrelation with coastal sea level (Figure 3). Local atmospheric forcing mechanisms that drive the relevant coastal sea level changes and Ekman transports across the open ocean at 26° N are tied to large-scale modes of surface atmospheric variation, namely, the NAO, Arctic Oscillation, and West Atlantic Index (Figure 4; cf. Figure S15).

Our interpretation is similar to the recent paradigm due to Volkov et al. (2018), whereby anticorrelation between the Atlantic overturning at 26° N and sea level across the Mediterranean Sea results from an analogous atmospheric teleconnection and local wind forcing. More broadly, by elucidating the anticorrelation between coastal sea level and the overturning circulation and the role of local atmospheric forcing, this study complements past papers establishing the importance of local air pressure and alongshore wind stress associated with large-scale climate modes as drivers of coastal sea level variability in this region on these timescales (Andres et al., 2013; Kenigson et al., 2018; Li et al., 2014; Noble, 1979; Piecuch & Ponte, 2015; Piecuch et al., 2016; Sandstrom, 1980; Thompson, 1986; Woodworth et al., 2014). Our findings clarify that anticorrelation observed between coastal sea level and the overturning circulation does not reflect a causal relationship in the sense of geostrophy, but rather arises from ageostrophic processes forced by temporally coherent, spatially separated local atmospheric forcing mechanisms. This contrasts with past studies, suggesting that anticorrelation between coastal sea level and the overturning circulation on interannual timescales results from purely geostrophic dynamics (Bingham & Hughes, 2009) or a direct causal relationship, such that the overturning circulation drives changes in coastal sea level (Goddard et al., 2015).

We should mention some caveats and open questions we are precluded from addressing due to space constraints. While local atmospheric forcing wholly explains the antiphase relationship observed between sea level and the overturning circulation, it only partially accounts for the variance in coastal tide-gauge data over the timescales and period of study. Moreover, large-scale teleconnection patterns only explain about half of the coastal sea level variance attributable to local wind and pressure forcing. Given the importance of understanding historical sea level observations for anticipating future coastal impacts, future studies should clarify the nature of these remaining coastal sea level variations and their underlying causes.

Our study was constrained by the availability of continuous overturning circulation measurements at 26° N since 2004. However, tide gauge data and reanalysis wind and pressure estimates are available for longer time periods (Compo et al., 2011; Laloyaux et al., 2016; Poli et al., 2013), and future studies should analyze relationships between New England sea level and Ekman transports across the subtropical Atlantic to see if similar results are found over longer periods going back in time. Such an analysis is timely, because the relationship between U.S. northeast coast sea level and the NAO is nonstationary—the two quantities are significantly correlated on interannual timescales during 1987–2012, but uncorrelated over 1970–1986 (Andres et al., 2013; Kenigson et al., 2018). Moreover, given the frequency dependence of the oceanic response to atmospheric forcing (e.g., Frankignoul et al., 1997), it is unclear to what extent our results for shorter periods apply more generally to longer timescales. For example, based on coupled climate model simulations, Little et al. (2017) find that, whereas alongshore wind stress is the dominant driver of coastal sea level variation on interannual timescales, significant coherence between New England sea level and the overturning circulation becomes apparent on decadal and longer timescales (cf. Frederikse et al., 2017; Woodworth et al., 2014). Given such nonstationarity and frequency dependence, we stress that our results apply strictly to the period and timescales studied, as other processes might be relevant for other time periods and frequency bands.

Finally, we considered the overturning circulation at 26° N, which is ~15–20° latitude south of New England. Our choice to focus on 26° N was made out of necessity, given the available overturning transport observations. Previous numerical and observational studies argue that, depending on timescale, overturning transports at one latitude in the Atlantic do not necessarily show in-phase coherence with overturning transports at other latitudes (Bingham et al., 2007; Elipot et al., 2014; Mielke et al., 2013). Thus, results shown here for the relationship between coastal sea level and the overturning at 26° N should not be taken as representative of how coastal sea level relates to the overturning at other latitudes. For example, Frederikse et al. (2017) show that, once local wind and pressure effects are removed from the tide gauge data and a low-pass filter is applied, U.S. northeast coast sea level is correlated with the variable thickness of Labrador Sea Water in the subpolar North Atlantic on decadal timescales during 1965–2014, perhaps indicating a relationship between coastal sea level and overturning at higher latitudes. Observational studies of

the relationship between coastal sea level and the overturning circulation at higher latitudes must await the accumulation of longer continuous circulation time series at other latitudes, emphasizing the importance of sustaining monitoring arrays that have recently come online (Lozier et al., 2017, 2019).

Acknowledgments
This work was supported by NSF awards OCE-1558966, OCE-1834739, and OCE-1805029; NASA contract NNH16CT01C; and the J. Lamar Worzel Assistant Scientist Fund and the Penzance Endowed Fund in Support of Assistant Scientists at the Woods Hole Oceanographic Institution. Helpful comments from Magdalena Andres and two anonymous reviewers are acknowledged. Tide-gauge sea level data were provided by the Permanent Service for Mean Sea Level (www.psmsl.org). Observations of the overturning circulation were taken from the RAPID data download page (www.rapid.ac.uk/data.php). Time series of the North Atlantic Oscillation and Arctic Oscillation were downloaded from the National Oceanic and Atmospheric Administration Earth System Research Laboratory Physical Sciences Division website (www.esrl.noaa.gov/psd/). Reanalysis wind stress and air pressure fields were provided by the Community Storage Server at Woods Hole Oceanographic Institution (http://cmip5.whoi.edu/).

References

Andres, M., Gawarkiewicz, G. G., & Toole, J. M. (2013). Interannual sea level variability in the western North Atlantic: Regional forcing and remote response. *Geophysical Research Letters*, *40*, 5915–5919. https://doi.org/10.1002/2013GL058013

Bingham, R. J., & Hughes, C. W. (2009). Signature of the Atlantic meridional overturning circulation in sea level along the east coast of North America. *Geophysical Research Letters*, *36*, L02603. https://doi.org/10.1029/2008GL036215

Bingham, R. J., Hughes, C. W., Roussenov, V., & Williams, R. G. (2007). Meridional coherence of the North Atlantic meridional overturning circulation. *Geophysical Research Letters*, *34*, L23606. https://doi.org/10.1029/2007GL031731

Buckley, M. W., & Marshall, J. (2016). Observations, inferences, and mechanisms of Atlantic Meridional Overturning Circulation variability: A review. *Reviews of Geophysics*, *54*, 5–63. https://doi.org/10.1002/2015RG000493

Compo, G. P., Whitaker, J. S., Sardeshmukh, P. D., Matsui, N., Allan, R. J., Yin, X., et al. (2011). The twentieth century reanalysis project. *Quarterly Journal of the Royal Meteorological Society*, *137*, 1–28. https://doi.org/10.1002/qj.776

Csanady, G. T. (1982). *Circulation in the Coastal Ocean* (pp. 281). Dordrecht, Holland: Springer.

Dee, D. P., Uppala, S. M., Simmons, A. J., Berrisford, P., Poli, P., Kobayashi, S., et al. (2011). The ERA-Interim reanalysis: Configuration and performances of the data assimilation system. *Quarterly Journal of the Royal Meteorological Society*, *137*, 553–597. https://doi.org/10.1002/qj.828

Elipot, S., Frajka-Williams, E., Hughes, C. W., & Willis, J. K. (2014). The observed north Atlantic meridional overturning circulation: Its meridional coherence and ocean bottom pressure. *Journal of Physical Oceanography*, *44*, 517–537. https://doi.org/10.1175/JPO-D-13-026.1

Frankignoul, C., Müller, P., & Zorita, E. (1997). A simple model of the decadal response of the ocean to stochastic wind forcing. *Journal of Physical Oceanography*, *27*, 1533–1546. https://doi.org/10.1175/1520-0485(1997)027<1533:ASMOTD>2.0.CO;2

Frederikse, T., Simon, K., Katsman, C. A., & Riva, R. (2017). The sea-level budget along the Northwest Atlantic coast: GIA, mass changes, and large-scale ocean dynamics. *Journal of Geophysical Research: Oceans*, *122*, 5486–5501. https://doi.org/10.1002/2017JC012699

Goddard, P. B., Yin, J., Griffies, S. M., & Zhang, S. (2015). An extreme event of sea-level rise along the Northeast coast of North America in 2009–2010. *Nature Communications*, *6*, 6346. https://doi.org/10.1038/ncomms7346

Grinsted, A., Moore, J. C., & Jevrejeva, S. (2004). Application of the cross wavelet transform and wavelet coherence to geophysical time series. *Nonlinear Processes in Geophysics*, *11*, 561–566. https://doi.org/10.5194/npg-11-561-2004

Heimbach, P., Wunsch, C., Ponte, R. M., Forget, G., Hill, C., & Utke, J. (2011). Timescales and regions of the sensitivity of Atlantic meridional volume and heat transport: Toward observing system design. *Deep-Sea Research*, *II*(58), 1858–1879. https://doi.org/10.1016/j.dsr2.2010.10.065

Holgate, S. J., Matthews, A., Woodworth, P. L., Rickards, L. J., Tamisiea, M. E., Bradshaw, E., et al. (2013). New data systems and products at the permanent service for mean sea level. *Journal of Coastal Research*, *29*(3), 493–504. https://doi.org/10.2112/JCOASTRES-D-12-00175.1

Hu, A., & Bates, S. C. (2018). Internal climate variability and projected future regional steric and dynamic sea level rise. *Nature Communications*, *9*, 1068. https://doi.org/10.1038/s41467-018-03474-8

Hurrell, J. W. (1995). Decadal trends in the North Atlantic Oscillation: Regional temperature and precipitation. *Science*, *269*(5224), 676–679. https://doi.org/10.1126/science.269.5224.676

Kalnay, E., Kanamitsu, M., Kistler, R., Collins, W., Deaven, D., Gandin, L., et al. (1996). The NCEP/NCAR 40-year reanalysis project. *Bulletin of the American Meteorological Society*, *77*(3), 437–471. https://doi.org/10.1175/1520-0477(1996)077<0437:TNYRP>2.0.CO;2

Kenigson, J. S., Han, W., Rajagopalan, B., Yanto, & Jasinski, M. (2018). Decadal shift of NAO-linked interannual sea level variability along the U.S. Northeast Coast. *Journal of Climate*, *31*, 4981–4989. https://doi.org/10.1175/JCLI-D-17-0403.1

Kistler, R., Kalnay, E., Collins, W., Saha, S., White, G., Woollen, J., et al. (2001). The NCEP-NCAR 50 year reanalysis: Monthly means CD-ROM and documentation. *Bulletin of the American Meteorological Society*, *82*, 247–267. https://doi.org/10.1175/1520-0477(2001)082<0247:TNNYRM>2.3.CO;2

Kopp, R. E. (2013). Does the mid-Atlantic United States sea level acceleration hot spot reflect ocean dynamic variability? *Geophysical Research Letters*, *40*, 3981–3985. https://doi.org/10.1002/grl.50781

Laloyaux, P., Balmaseda, M., Dee, D., Mogensen, K., & Janssen, P. (2016). A coupled data assimilation system for climate reanalysis. *Quarterly Journal of the Royal Meteorological Society*, *142*, 65–78. https://doi.org/10.1002/qj.2629

Landerer, F. W., Jungclaus, J. H., & Marotzke, J. (2007). Regional dynamic and steric sea level change in response to the IPCC-A1B Scenario. *Journal of Physical Oceanography*, *37*, 296–312. https://doi.org/10.1175/JPO3013.1

Li, Y., Ji, R., Fratantoni, P. S., Chen, C., Hare, J. A., Davis, C. S., & Beardsley, R. C. (2014). Wind-induced interannual variability of sea level slope, along-shelf flow, and surface salinity on the Northwest Atlantic shelf. *Journal of Geophysical Research: Oceans*, *119*, 2462–2479. https://doi.org/10.1002/2013JC009385

Little, C. M., Piecuch, C. G., & Ponte, R. M. (2017). On the relationship between the meridional overturning circulation, alongshore wind stress, and United States East Coast sea level in the Community Earth System Model Large Ensemble. *Journal of Geophysical Research: Oceans*, *122*, 4554–4568. https://doi.org/10.1002/2017JC012713

Lozier, M. S., Bacon, S., Bower, A. S., Cunningham, S. A., de Jong, M. F., de Steur, L., et al. (2017). Overturning in the Subpolar North Atlantic Program: A new international ocean observing system. *Bulletin of the American Meteorological Society*, *98*(4), 737–752. https://doi.org/10.1175/BAMS-D-16-0057.1

Lozier, M. S., Li, F., Bacon, S., Bahr, F., Bower, A. S., Cunningham, S. A., et al. (2019). A sea change in our view of overturning in the subpolar North Atlantic. *Science*, *363*(6426), 516–521. https://doi.org/10.1126/science.aau6592

McCarthy, G. D., Smeed, D. A., Johns, W. E., Frajka-Williams, E., Moat, B. I., Rayner, D., et al. (2015). Measuring the Atlantic meridional overturning circulation at 26° N. *Progress in Oceanography*, *130*, 91–111. https://doi.org/10.1016/j.pocean.2014.10.006

Mielke, C., Frajka-Williams, E., & Baehr, J. (2013). Observed and simulated variability of the AMOC at 26° N and 41° N. *Geophysical Research Letters*, *40*, 1159–1164. https://doi.org/10.1002/grl.50233

Noble, M. (1979). Low-frequency wind-induced sea level oscillations along the east coast of North America. *Journal of Geophysical Research*, *84*(C6), 3227–3236. https://doi.org/10.1029/JC084iC06p03227

Permanent Service for Mean Sea Level (PSMSL) (2018). Tide gauge data. Retrieved 3 December, 2018 https://doi.org/http://www.psmsl.org/data/obtaining/

Piecuch, C. G., Dangendorf, S., Ponte, R. M., & Marcos, M. (2016). Annual sea level changes on the North American Northeast Coast: Influence of local winds and barotropic motions. *Journal of Climate*, *29*, 4801–4816. https://doi.org/10.1175/JCLI-D-16-0048.1

Piecuch, C. G., & Ponte, R. M. (2015). Inverted barometer contributions to recent sea level changes along the northeast coast of North America. *Geophysical Research Letters*, *42*, 5918–5925. https://doi.org/10.1002/2015GL064580

Piecuch, C. G., Ponte, R. M., Little, C. M., Buckley, M. W., & Fukumori, I. (2017). Mechanisms underlying recent decadal changes in subpolar North Atlantic Ocean heat content. *Journal of Geophysical Research: Oceans*, *122*, 7181–7197. https://doi.org/10.1002/2017JC012845

Pillar, H. R., Heimbach, P., Johnson, H. L., & Marshall, D. P. (2016). Dynamical attribution of recent variability in Atlantic overturning. *Journal of Climate*, *29*, 3339–3352. https://doi.org/10.1175/JCLI-D-15-0727.1

Poli, P., Hersbach, H., Tan, D., Dee, D., Thépaut, J.-N., Simmons, A., et al. (2013). The data assimilation system and initial performance evaluation of the ECMWF pilot reanalysis of the 20th-century assimilating surface observations only (ERA-20C). ERA report series 14 62.

Sallenger, A. H., Doran, K. S., & Howd, P. A. (2012). Hotspot of accelerated sea-level rise on the Atlantic coast of North America. *Nature Climate Change*, *2*, 884–888. https://doi.org/10.1038/nclimate1597

Sandstrom, H. (1980). On the wind-induced sea level changes on the Scotian Shelf. *Journal of Geophysical Research*, *85*, 461–468. https://doi.org/10.1029/JC085iC01p00461

Thompson, K. R. (1986). North Atlantic sea-level and circulation. *Geophysical Journal of the Royal Astronomical Society*, *87*(1), 15–32. https://doi.org/10.1111/j.1365-246X.1986.tb04543.x

Thompson, D. W. J., & Wallace, J. M. (1998). The Arctic oscillation signature in the wintertime geopotential height and temperature fields. *Geophysical Research Letters*, *25*(9), 1297–1300. https://doi.org/10.1029/98GL00950

Volkov, D. L., Baringer, M., Smeed, D., Johns, W., & Landerer, F. W. (2018). Teleconnection between the Atlantic meridional overturning circulation and sea level in the Mediterranean Sea. *Journal of Climate*, *32*(3), 935–955. https://doi.org/10.1175/JCLI-D-18-0474.1

Woodworth, P. L., Maqueda, A., Roussenov, V., Williams, R. G., & Hughes, C. W. (2014). Mean sea-level variability along the northeast American Atlantic coast and the roles of the wind and the overturning circulation. *Journal of Geophysical Research: Oceans*, *119*, 8916–8935. https://doi.org/10.1002/2014JC010520

Wunsch, C., & Stammer, D. (1997). Atmospheric loading and the oceanic "inverted barometer" effect. *Reviews of Geophysics*, *35*(1), 79–107. https://doi.org/10.1029/96RG03037

Yin, J., Schlesinger, M. E., & Stouffer, R. J. (2009). Model projections of rapid sea-level rise on the northeast coast of the United States. *Nature Geoscience*, *2*, 262–266. https://doi.org/10.1038/ngeo462

Zhao, J., & Johns, W. (2014). Wind-forced interannual variability of the Atlantic meridional overturning circulation at 26.5° N. *Journal of Geophysical Research: Oceans*, *119*, 2403–2419. https://doi.org/10.1002/2013JC009407